ELSEVIER

Chemical Engineering Journal 83 (2001) 95–105

Chemical Engineering Journal

www.elsevier.com/locate/cej

On the importance of non-ideal flow effects in the operation of industrial-scale adiabatic membrane reactors

M.K. Koukou, N. Papayannakos, N.C. Markatos*

Department of Chemical Engineering, National Technical University of Athens, 9, Heroon Polytechniou Street, Zografou Campus, GR-15780 Zografou, Athens, Greece

Received 20 September 1999; received in revised form 12 July 2000; accepted 17 July 2000

Abstract

A mathematical model taking into account mass dispersion is presented for the simulation of the performance of an adiabatic full-scale membrane reactor. Results are presented from the application of this model to a membrane reactor, that is introduced in an integrated gasification combined cycle plant, to control carbon dioxide emissions. The performance of this reactor equipped with highly selective membranes is studied in detail. The extent of the impact of the non-ideal flow effects on the membrane reactor operation is discussed. It is shown that dispersion effects have a negative influence on the performance of industrial-scale membrane reactors and they must be considered as a basic parameter to their design. © 2001 Elsevier Science B.V. All rights reserved.

Keywords: Membrane; Non-ideal flow; Industrial-scale; Module design

1. Introduction

The membrane reactor concept appeared for the first time in the early 1950s but a lot of applications have emerged in the last two decades due to the significant developments in membrane materials and modules. These devices have been proposed for various applications and they are especially used for reactions the yields of which are limited by thermodynamic equilibrium. Nowadays, membrane reactor technology proposes an alternative solution to conventional reactors [1–5]. Large industrial membrane reactors will be composed in many cases of banks of tubular ceramic membranes. The use of ceramic membranes in these reactors is recommended primarily due to their thermal and mechanical stability [1]. The various assumptions made in modelling their behaviour (e.g. plug flow conditions, isothermal conditions) should be checked and when not valid more complicated models have to be developed for the realistic simulation of such systems [5]. In many cases, the optimum performance of a membrane reactor requires a highly selective ceramic membrane for the selective removal of a product, mainly hydrogen.

In a recent work, the performance of a laboratory-scale isothermal membrane reactor has been simulated [6,7] and a significant influence of the non-ideal flow effects on the reactor operation has been confirmed. The reaction of dehydrogenation of cyclohexane was considered as a model reaction in those works. The effect of the non-isothermal conditions prevailing in experimental membrane reactors on their performance is discussed in another work [8]. A first attempt on developing simulation tools for the design of industrial-scale membrane reactors has been recently published [9,10], where plug flow conditions were assumed on both sides of the membrane reactor.

In the present work, a mathematical model is presented for the simulation of the operation of a full-scale adiabatic membrane reactor taking into account mass dispersion on both sides of the membrane. The water gas shift (WGS) reaction is considered to take place on the feed side of the membrane reactor which is filled with catalyst particles. This reactor is a major part of an integrated gasification combined cycle (IGCC) plant for the decrease and control of carbon dioxide emissions [9]. Two versions of the model are used. The first one, called the dispersion model (DM), accounts for the dispersion effects inside the reactor while the second one, called the simplified model (SM), assumes plug flow conditions inside the reactor. The results obtained from those two versions of the model are compared for the purpose of investigating the possible influence of dispersion effects on the industrial-scale membrane reactor performance.

* Corresponding author. Tel.: +301-772-3126; fax: +301-772-3228.
E-mail address: n.markatos@ntua.gr (N.C. Markatos).

1385-8947/01/$ – see front matter
PII: S1385-8947(00)00243-6

Nomenclature

A_{ki}	constants for the calculation of species specific heats
c_i	mass fraction ($kg_i\ kg^{-1}$)
C_p	mixture specific heat ($J\ kg^{-1}\ K^{-1}$)
c_{pi}	component specific heat ($J\ mol^{-1}\ K^{-1}$)
D_a	axial dispersion coefficient ($m^2\ s^{-1}$)
d_e	equivalent diameter (m)
d_p	particle diameter (m)
D_r	radial dispersion coefficient ($m^2\ s^{-1}$)
d_t	tube diameter (m)
h_f, h_s	heat transfer coefficients between the membrane surface and the fluid in contact, on the feed and separation side, respectively ($W\ m^{-2}\ K^{-1}$)
k_r	constant of reaction rate ($((dm^3)^{\alpha}\ kg^{-1}\ s^{-1}\ mol^{-\alpha}$)
k	membrane thermal conductivity ($W\ m^{-1}\ K^{-1}$)
L	length of catalytic bed (m)
MW	mixture mean molecular weight ($kg\ mol^{-1}$)
Pe_a	axial Peclet number
Pe_r	radial Peclet number
P_f	total pressure on the feed side (Pa)
P_s	total pressure on the separation side (Pa)
Q_f	inlet specific feed rate ($kg\ m^{-2}\ s^{-1}$)
$Q_{f,m}$	inlet feed rate ($mol\ s^{-1}$)
Q_i	separation rate of component i ($kg\ m^{-2}\ s^{-1}$)
Q_s	inlet specific sweep gas rate ($kg\ m^{-2}\ s^{-1}$)
$Q_{s,m}$	inlet sweep gas rate ($mol\ s^{-1}$)
r	radial coordinate in Eqs. (1a)–(1e) (m)
r	sweep ratio, $Q_{s,m}/Q_{f,m}$
R	reactor radius $0 < R < R_{out}$ (m)
R_{in}	inner radius of the membrane tubes (m)
R_{mem}	outer radius of the membrane tubes (m)
R_{out}	outer radius of the membrane reactor (m)
S_{c_i}	sink or source in Eq. (1d)
S_h	sink or source in Eq. (1e)
S_{u_r}	sink or source in Eq. (1b)
S_{u_z}	sink or source in Eq. (1c)
T_1	reference temperature equal to $298\ K = 77^{\circ}F$
T_2	inlet temperature (°F)
u_r	radial velocity in Eq. (1b) ($m\ s^{-1}$)
u_s	superficial velocity ($m\ s^{-1}$)
u_z	axial velocity in Eq. (1c) ($m\ s^{-1}$)
x_i	molar fraction of the component i on the feed side
y_i	molar fraction of the component i on the separation side
z	axial coordinate (m)
[]	concentration of component i ($mol\ m^{-3}$)

Greek symbol

α_i	permeability coefficient of component i ($kg\ m^{-2}\ s^{-1}\ Pa^{-1}$)
β	reversibility factor $[CO][H_2O]/[CO_2][H_2]$
ΔH_f^0	heat of formation, calculated equal to $-41\,192\ J\ mol^{-1}$
Δp	pressure drop (Pa)
ε	bed porosity (−)
λ	mixture thermal conductivity ($W\ m^{-1}\ K^{-1}$)
μ	laminar viscosity (Pa s)
μ_b	viscosity at bulk temperature (Pa s)
μ_w	viscosity at wall temperature (Pa s)
ν_i	stoichiometric coefficients in water gas shift reaction
Φ_L	dimensionless reactor length $= z/L$
Φ_R	dimensionless reactor radius $= R/R_{out}$

2. Process design aspects

Tubular systems are considered as state of the art in membrane technology as they have the best performance combined with aspects of desired attainable surface area and module construction [1,9]. A multi-tubular full-scale WGS membrane reactor has been reported recently [9], introduced in an IGCC plant, to increase energy efficiency and control CO_2 emissions. Conventional CO_2 removal process schemes for oxygen blown entrained bed gasifiers comprise low temperature gas cleaning, a separate WGS conversion step, to convert CO with steam in the fuel gas mixture into CO_2 and H_2, followed by CO_2 removal. The extent of the WGS conversion determines the final CO concentration in the fuel gas and thus the maximum level of CO_2 control. The implementation of a catalytic membrane reactor, in which the WGS reaction is combined with H_2 separation from the reaction mixture in one reactor, using ceramic membranes selectively permeable to hydrogen, is a possible way to increase the WGS conversion [9]. Inorganic highly selective membranes are necessary because of the high temperature level at which the reaction occurs (300–500°C). Data on the permeation and selectivity of the membrane have been obtained in laboratory-scale experiments [9].

3. Simulation of the industrial WGS membrane reactor

3.1. The physical problem

The simulation of the performance of the proposed complicated full WGS-MR is achieved by considering the reactor as an annulus where the diameter of the outer tube (shell) is equivalent to the distance between two neighbouring membrane tubes of the full-scale WGS-MR [10]. The feed gas enters the space between the two tubes where the catalyst is placed (feed side) and the exothermic WGS reaction takes place, while a sweep gas enters the membrane

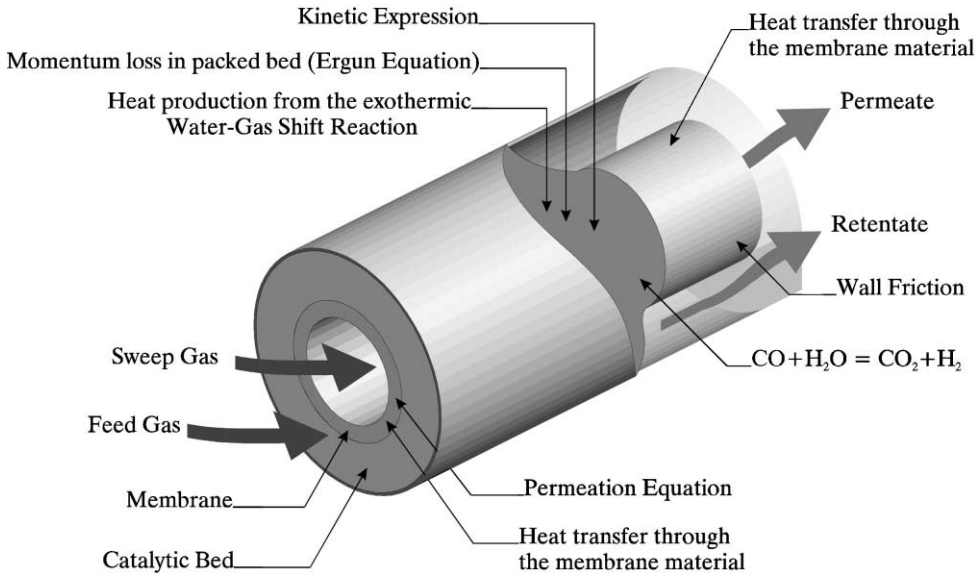

Fig. 1. Schematic description of the system studied.

tube sweeping the permeated gases to the outlet (separation side), either in co-current or in counter-current flow with the feed gas (Fig. 1).

3.2. Mathematical formulation and numerical solution

Heat dispersion effects on both feed and separation sides have been checked to have very little influence on the results [8]. Details on the development of the mathematical model are described elsewhere [10]. Adiabatic operation is considered for both the two versions of the numerical code used. In the simplified model, plug flow conditions were applied, while in the dispersion model non-ideal flow effects were taken into account, with dispersion coefficient values found in the literature [11,12], as listed in Table 1.

The mathematical analysis is based on a set of elliptic, partial differential equations expressing the conservation of mass, momentum, chemical species and enthalpy in steady, two-dimensional flow [10]. It is assumed that there is no angular variation of the dependent variables and there obviously exists flow symmetry. The dependent variables are the total pressure, P ($\mathrm{N\,m^{-2}}$), the radial and axial velocity components, u_r, u_z ($\mathrm{m\,s^{-1}}$), the mass fractions of chemical species, c_i ($\mathrm{kg_i\,kg^{-1}}$), and the mixture specific enthalpy, h ($\mathrm{J\,kg^{-1}}$), while their differential equations are expressed as follows:

$$\text{Continuity}: \quad \frac{1}{r}\frac{\partial}{\partial r}(r\rho u_r) + \frac{\partial}{\partial z}(\rho u_z) = 0 \tag{1a}$$

$$r\text{-momentum}: \quad \frac{1}{r}\frac{\partial}{\partial r}(r\rho u_r^2) + \frac{\partial}{\partial z}(\rho u_z u_r) - \frac{1}{r}\frac{\partial}{\partial r}\left(r\mu\frac{\partial u_r}{\partial r}\right) - \frac{\partial}{\partial z}\left(\mu\frac{\partial u_r}{\partial z}\right) = S_{u_r} \tag{1b}$$

$$z\text{-momentum}: \quad \frac{1}{r}\frac{\partial}{\partial r}(r\rho u_r u_z) + \frac{\partial}{\partial z}(\rho u_z^2) - \frac{1}{r}\frac{\partial}{\partial r}\left(r\mu\frac{\partial u_z}{\partial r}\right) - \frac{\partial}{\partial z}\left(\mu\frac{\partial u_z}{\partial z}\right) = S_{u_z} \tag{1c}$$

$$\text{Mass fraction } c_i: \quad \frac{1}{r}\frac{\partial}{\partial r}(r\rho u_r c_i) + \frac{\partial}{\partial z}(\rho u_z c_i) - \frac{1}{r}\frac{\partial}{\partial r}\left(r\rho D_r\frac{\partial c_i}{\partial r}\right) - \frac{\partial}{\partial z}\left(\rho D_\mathrm{a}\frac{\partial c_i}{\partial z}\right) = S_{c_i} \tag{1d}$$

Table 1
Dispersion coefficient values used in the modelling

	Axial dispersion coefficient	Radial dispersion coefficient
Feed side	$Pe_\mathrm{a} = \frac{u_z d_\mathrm{p}}{D_\mathrm{a}} = 2 \Leftrightarrow D_\mathrm{a} = u_z\frac{d_\mathrm{p}}{2}$	$Pe_r = \frac{u_z d_\mathrm{p}}{D_r} = 10 \Leftrightarrow D_r = u_z\frac{d_\mathrm{p}}{10}$
Separation side	$Pe_\mathrm{a} = \frac{u_z d_\mathrm{p}}{D_\mathrm{a}} = 10 \Leftrightarrow D_\mathrm{a} = u_z\frac{d_\mathrm{p}}{10}$	$Pe_r = \frac{u_z d_\mathrm{p}}{D_r} = 10^3 \Leftrightarrow D_r = u_z\frac{d_\mathrm{p}}{10^3}$

$$\text{Enthalpy } h: \quad \frac{1}{r}\frac{\partial}{\partial r}(r\rho u_r h) + \frac{\partial}{\partial z}(\rho u_z h) - \frac{1}{r}\frac{\partial}{\partial r}\left(r\frac{\lambda}{C_p}\frac{\partial h}{\partial r}\right) - \frac{\partial}{\partial z}\left(\frac{\lambda}{C_p}\frac{\partial h}{\partial z}\right) = S_h \tag{1e}$$

where ρ is the mixture density (kg m^{-3}), μ the laminar viscosity (Pa s), D_a and D_r are the axial and radial dispersion coefficient values describing diffusive fluxes (m^2 s^{-1}), λ the mixture thermal conductivity (W m^{-1} K^{-1}), and C_p the mixture specific heat (J kg^{-1} K^{-1}). The terms S_{u_r}, S_{u_z}, S_{c_i}, and S_h express various sources (e.g. pressure gradient for the momentum equations, reaction source and separation source for the mass fraction equations, enthalpy source for the energy equation) for the respective variable inside the domain of interest.

The set of the partial differential equations for the various dependent variables, in conjunction with the appropriate boundary and internal conditions describing the physical problem considered, has been solved using the SIMPLEST algorithm embodied in the general PHOENICS® package [13–15].

3.3. Geometry — grid development

A polar–cylindrical coordinate system is used and the dimensions of the membrane tubes together with the distance between them inside the module studied are presented in Table 2. The choice of the grid size was dictated by performing grid independence studies and a grid consisting of 11×50 ($N_y \times N_z$) cells was proved adequate for the simplified model runs. In the dispersion runs, a grid of 31×50 cells was found to be adequate to describe the physical problem studied. In the latter case, the grid was non-uniform in the radial direction and was finer close to the membrane because of the presence of partial pressure gradients there.

3.4. Boundary — internal conditions

3.4.1. Inlet–outlet

Inlet flow rates and values for all dependent variables are specified on both sides of the system. The applied inlet specific feed rates ranged from 1.0 to 2.5 kg m^{-2} s^{-1}. The inlet sweep gas rates were based on the sweep ratio (which is the ratio of the molar inlet sweep gas rate to the molar inlet feed rate), and five sweep ratios were applied ($r = 0.52, 0.72, 0.92, 1.12, 1.32$). In Table 3, the conditions used in the simulations are presented, while Table 4 shows the respective compositions. A pressure drop of 15 bar across the membrane is necessary to obtain the required driving force for hydrogen transport through the membrane. The temperature at the inlets of the reactor was set to 598 K based on considerations of best IGCC performance [9].

Table 2
Geometrical characteristics used in the simulations

Distance between the membrane tubes (m)	6E−2
Outer diameter of the membrane tube (m)	1.4E−2
Inner diameter of the membrane tube (m)	8E−3
Reactor length (m)	2

Table 3
Conditions used in the simulations

Flow mode	Co-current
Feed side pressure (bar)	36
Separation side pressure (bar)	21
Inlet temperature on the feed side (K)	598
Inlet temperature on the separation side (K)	598

Table 4
Inlet composition used in the simulations

	H_2	CO	H_2O	CO_2	N_2
Feed side (mol mol^{-1})	0.3873	0.1288	0.2273	0.2431	0.0135
Separation side (mol mol^{-1})	–	–	0.113	–	0.887

At the outlet, the external pressure is assumed radially uniform and the computed pressures are relative to the outlet pressure. The values of all variables are properly calculated at both outlets because of the upwind interpolation [13,15].

3.4.2. Wall friction

The no-slip condition was used for velocities and the fluid-to-wall friction losses were properly computed by the log-law functions at all walls [15]. The axial velocity was equal to zero at the walls of the cylinders [15,16]. To avoid use of very fine grids close to walls, special frictional sources were applied in the momentum equations equal to $-u_z A\mu/y$, where μ is the mixture viscosity, A the surface, u_z the axial velocity parallel to the surface and y the distance from the cell centre to the wall.

3.4.3. Symmetry plane boundary conditions

Zero-flux conditions were applied at the symmetry plane for all variables.

3.4.4. Gas permeation equation

The evaluations were based on the characteristics of highly selective microporous silica membranes, although their stability under WIHYS conditions is under investigation [9,17,18]. These membranes show a good combination of permeability and selectivity. The selectivity of H_2/CO_2 is about 15 and the permeability of hydrogen is equal to 2×10^{-6} mol m^{-2} Pa^{-1} s^{-1}. The gas permeation equation used to describe the permeation rate of the chemical species through these membranes is

$$Q_i = \alpha_i (x_i P_f - y_i P_s) \tag{2}$$

where Q_i is the separation rate of component i (kg m^{-2} s^{-1}), α_i the permeability coefficient of component i (kg m^{-2} s^{-1} Pa^{-1}), x_i the molar fraction of the component i on the feed side, y_i the molar fraction of the component i on the separation side, P_f the total pressure on the feed side (Pa), and P_s the total pressure on the separation side (Pa). Mass transfer resistance has been checked to be negligible at the conditions studied.

3.4.5. Reaction kinetics

Based on the results of a literature survey, a Fe–Cr catalyst appears to fit best the application of WGS, and the following power-law type rate expression was preferred [19] extrapolated to the feed side pressure:

$$r = k_r[CO]^{0.73}[H_2O]^{0.55}[CO_2]^0[H_2]^0(1-\beta) \quad (3)$$

where k_r is the constant of reaction rate and β the reversibility factor equal to $[CO][H_2O]/[CO_2][H_2]$.

3.4.6. Momentum loss in catalytic bed

The well-known Ergun equation was used to describe the momentum loss in the packed bed in terms of pressure gradient [16]:

$$\frac{\Delta p}{L} = 150\frac{(1-\varepsilon)^2\mu u_s}{\varepsilon^3 d_p^2} + 1.75\frac{(1-\varepsilon)u_s^2\rho}{\varepsilon^3 d_p} \quad (4)$$

where Δp is the pressure drop (Pa), L the length of catalytic bed (m), ε the bed porosity (−), μ the laminar viscosity, and u_s the superficial velocity.

3.5. Computational details

The simulation runs were performed on a Silicon Graphics R4000 XS24 Indigo Workstation and convergence was achieved by applying under-relaxation techniques. About 2000 sweeps of the computational domain were needed for the simplified model to assure full convergence, when using a grid of 11 × 50 cells. In the case of the dispersion model, because of the finer grid used, about 4000 sweeps of the computational domain were needed to achieve full convergence. Each sweep requires for the latter case 2.0 s CPU time.

3.6. Estimation of thermal properties

The thermal properties required for the formulation of the basic conservation equations for the heat transport through the membrane walls are presented in Table 5.

4. Results and discussion

The main objective of this research work was to investigate whether the non-ideal flow effects influence the performance of an industrial adiabatic membrane reactor in which highly selective ceramic membranes were embodied.

The results from the application of the developed mathematical model in a WGS membrane reactor are presented in terms of reactor conversion and hydrogen recovery, as defined in Table 6. In parts a and b of Figs. 2 and 3, membrane reactor conversion and hydrogen recovery values are presented for a wide range of sweep ratios r and inlet feed rates. The predictions are obtained by using two versions of the developed mathematical model: the *simplified model* which assumes plug flow conditions on both sides of the system considered and the *dispersion model* which takes into account the non-ideal flow effects on both sides of the WGS-MR. It is easily noticed, by studying the above figures, that the influence of the dispersion effects on the reactor performance is negative, as the CO conversion and hydro-

Table 5
Estimation of thermal properties

(1) Specific heat of the mixture, C_p (J kg^{-1} K^{-1}) [20]: $C_p = (4.19\text{MW})\left[\sum x_i A_{1i} + \sum x_i A_{2i} T + \sum x_i A_{3i} T^2\right]$, where MW is the mixture mean molecular weight, and A_{ki} the constants for the calculation of species specific heats

(2) Heat of reaction, ΔH (J mol^{-1}) [21]: $\Delta H = \Delta H_f^0 + \int \nu_i c_{pi}\,dT$, where ΔH_f^0 is the arithmetic sum of heats of formation of reaction components, calculated equal to −41 192 J mol^{-1}, and ν_i the stoichiometric coefficients in water gas shift reaction

(3) Mixture thermal conductivity, λ (W m^{-1} K^{-1}) and membrane thermal conductivity k (W m^{-1} K^{-1}): values of λ are calculated by $\lambda = \Sigma x_i \lambda_i$, where λ_i is the thermal conductivities (W m^{-1} K^{-1}) of various gases, calculated at $P = 36$ and 21 bar using two methods: (i) Stiel and Thodos and (ii) Chung [21]. In the modelling of the non-isothermal adiabatic membrane reactor, a relationship $\lambda = f(T)$ is used to account for the variation of thermal conductivity with temperature at high pressures. Membrane thermal conductivity k is calculated from the literature and a relationship $k = f(T)$ is used [22]

(4) Heat transfer coefficients between the membrane wall and the fluid (W m^{-2} K^{-1}):

Feed side: The following relationship was used [21]: $hd_p/\lambda = 3.6(d_p G/\mu\varepsilon)^{0.365}$, where h is the heat transfer coefficient (W m^{-2} K^{-1}), d_p the particle diameter equal to 3.55E−3 (m), λ the mixture thermal conductivity (W m^{-1} K^{-1}), G the superficial velocity (m s^{-1}) and ε the bed porosity equal to 0.38 (−)

Separation side: In the region $2000 < Re < 10\,000$, which usually is the case in the modelling, Hausen's equation was used [21]: $hd_t/\lambda = 0.116(N_{Re}^{2/3} - 125)N_{Pr}^{1/3}[1 + (d_t/L)^{2/3}](\mu_b/\mu_w)^{0.14}$, where d_t is the tube diameter (m), λ the mixture thermal conductivity (W m^{-1} K^{-1}), N_{Re} the Reynolds number $= u_z D_t/\mu$ (−), N_{Pr} the Prandtl number $= c_p\mu/\lambda$ (−), L the reactor length (m), μ_b the viscosity at bulk temperature (Pa s), and μ_w the viscosity at wall temperature (Pa s)

Inlet enthalpy values (J kg^{-1}): $H_{in} = \int_{T_2}^{T_1} \sum x_i c_{pi}\,dT$, where T_1 is the reference temperature equal to 298 K = 77°F, T_2 the inlet temperature (°F), and c_{pi} the component specific heat

Table 6
Membrane reactor parameters

Membrane reactor parameter	Definition	Description
CO conversion	CO converted/CO entering	Fraction of CO entered that has reacted
H_2 recovery	H_2 in permeate/H_2 + CO entering	Fraction of H_2, of the maximum theoretical amount that can be formed, recovered in the permeate stream

gen recovery predicted by the dispersion model are always much lower than the respective values predicted by the simplified model. When the inlet specific feed rate increases, a decrease in the membrane reactor conversion and hydrogen recovery values is predicted by both models. When the sweep ratio r and thus the sweep gas rate increases, both the membrane reactor conversion and the hydrogen recovery increase. This behaviour is due to the impact of the sweep gas flow on the hydrogen fluxes through the membrane. As the sweep flow increases, the hydrogen concentration and partial pressure decrease on the separation side, resulting in an increased hydrogen partial pressure difference which acts as the driving force for the separation through the membrane.

In parts a and b of Figs. 4 and 5, axial profiles of hydrogen partial pressure are shown on both sides of the membrane reactor for various sweep ratios r, as predicted by the simplified and the dispersion models. For the simplified model, the values correspond to uniform partial pressure along the reactor radius, while for the dispersion model they correspond to the closest to the membrane tube wall grid point ($\Phi_R = 0.245$ and 0.132 for the feed and separation side, respectively). The simplified model predicts a maximum of hydrogen partial pressure close to the reactor inlet, and then a decrease up to the reactor outlet (Fig. 4a). This initial increase of the hydrogen partial pressure is explained by considering the difference between the high initial reaction rates, that produce large quantities of hydrogen, and the amount of hydrogen separated through the highly selective membrane from the feed to the separation side. This difference is positive close to inlet and increases up to the maximum

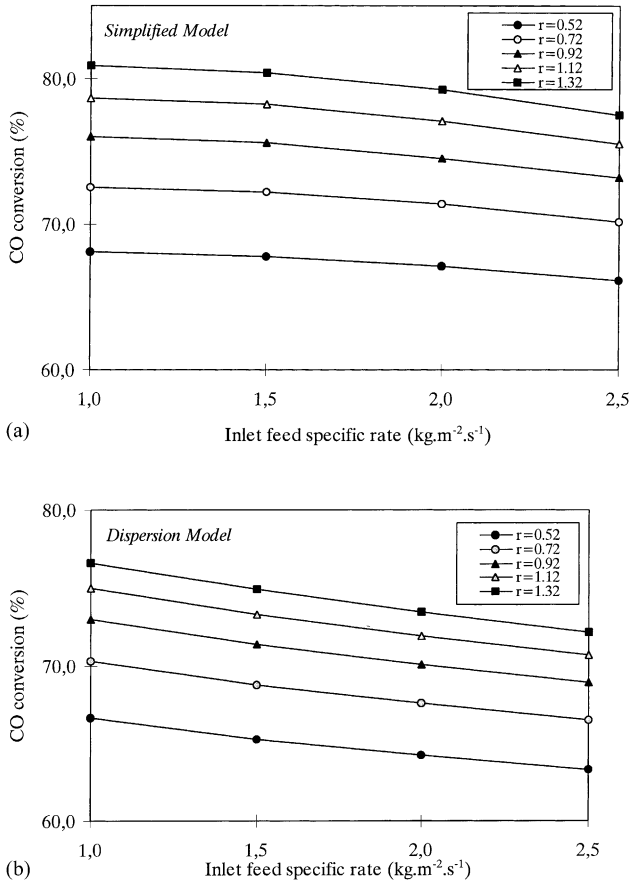

Fig. 2. Membrane reactor CO conversion vs. inlet specific feed rate for various sweep ratios r for (a) simplified model and (b) dispersion model.

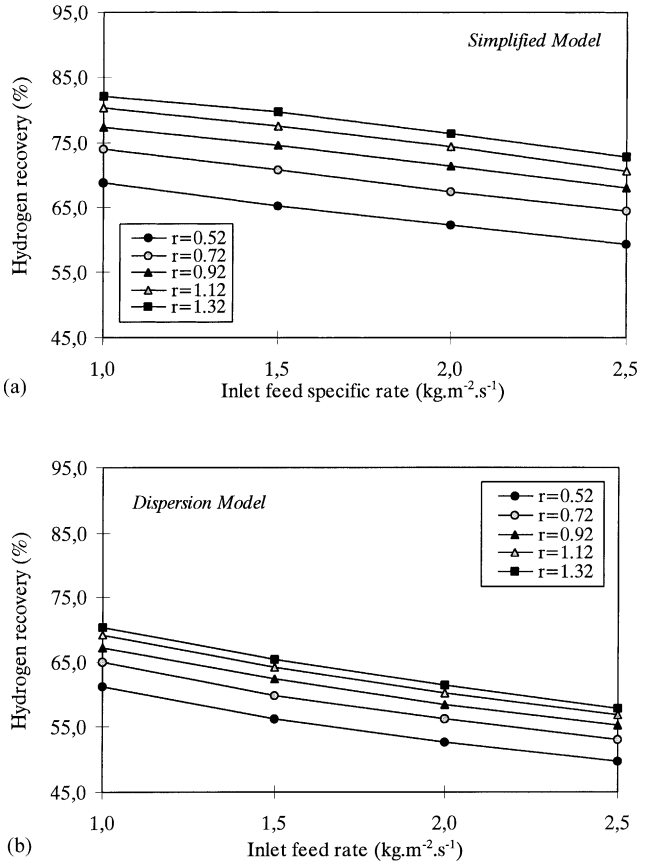

Fig. 3. Hydrogen recovery vs. inlet specific feed rate for various sweep ratios r for (a) simplified model and (b) dispersion model.

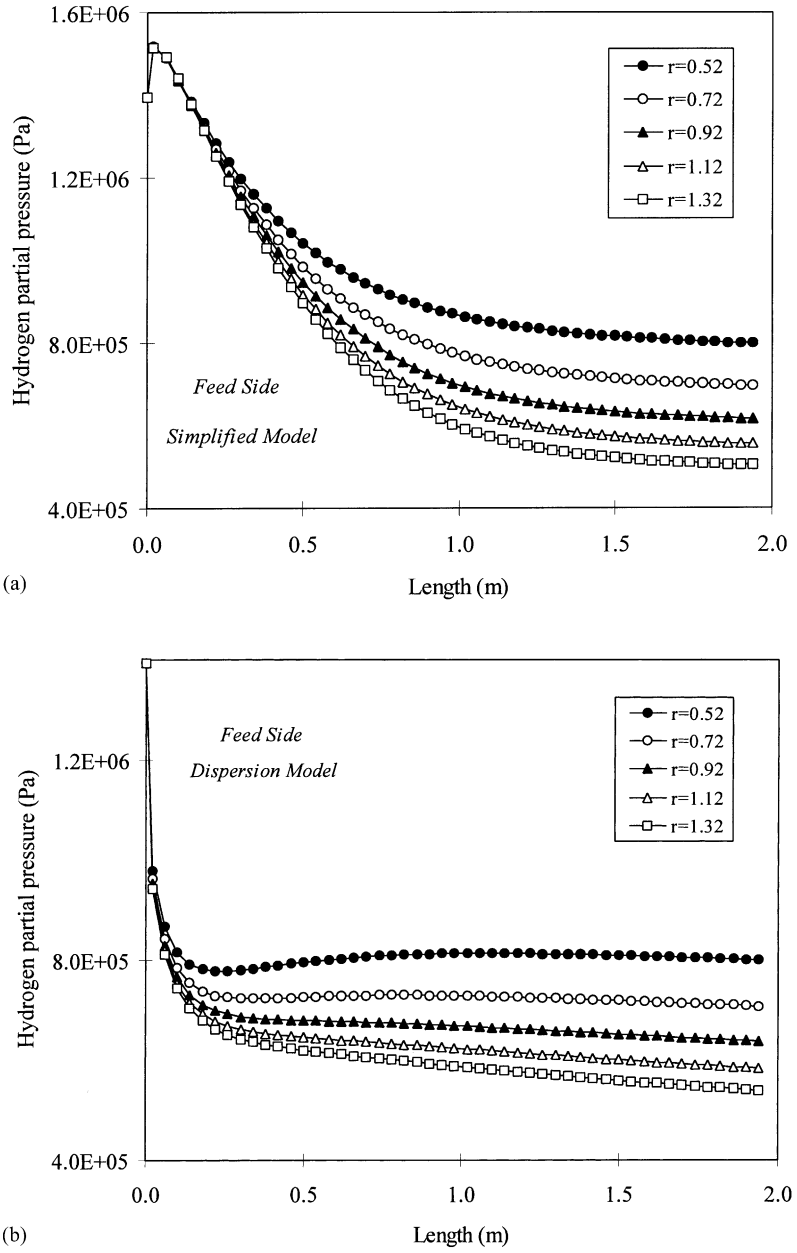

Fig. 4. Axial profiles of hydrogen partial pressure on the feed side for various sweep ratios r for (a) simplified model inlet specific feed rate $= 1.0\,\mathrm{kg\,m^{-2}\,s^{-1}}$) and (b) dispersion model ($\Phi_R = 0.246$, inlet specific feed rate $= 1.0\,\mathrm{kg\,m^{-2}\,s^{-1}}$).

but thereafter it decreases continuously as the reaction rates diminish because of the depletion of reactants CO and H_2O, while hydrogen is transported through the membrane on the separation side. When the inlet sweep gas rate increases, the amount of hydrogen removed from the feed side increases, because of the increased partial hydrogen pressure difference between the feed and separation side streams, and the hydrogen partial pressure on the feed side decreases. The dispersion model predicts a steep initial decrease of hydrogen partial pressure close to the membrane wall (Fig. 4b), which is attributed to the difference between the quantity of hydrogen removed from the wall through the membrane and the hydrogen supplied from the bulk of the gas, via the dispersion fluxes. Following the initial steep decrease, hydrogen partial pressure decreases very slowly after $L = 0.15\,\mathrm{m}$ for $r = 0.92$–1.32, while for $r = 0.52$–0.72 it follows a slight increase as the result of the diminished amount of hydrogen transported through the membrane, compared to the amount supplied from the bulk of the gas on the feed side. On the separation side, the hydrogen partial pressure increases along the reactor length, because of hydrogen separation through the membrane (Figs. 5a and b). Increase in the sweep ratio r and in the inlet sweep gas rate result in dilution of the hydrogen transported through the membrane

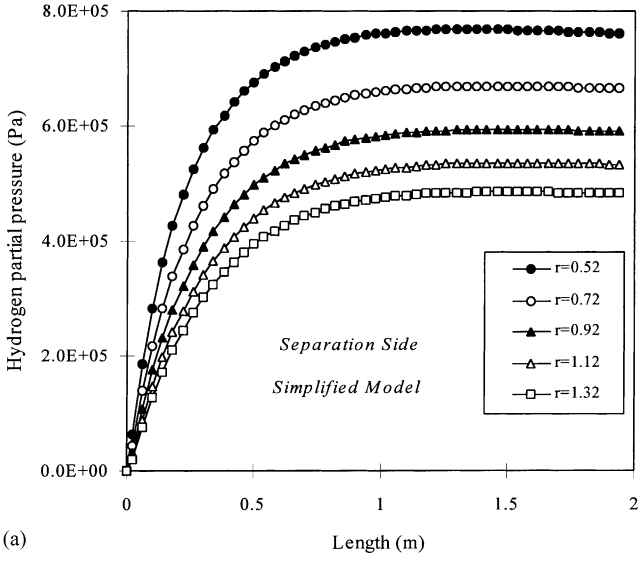

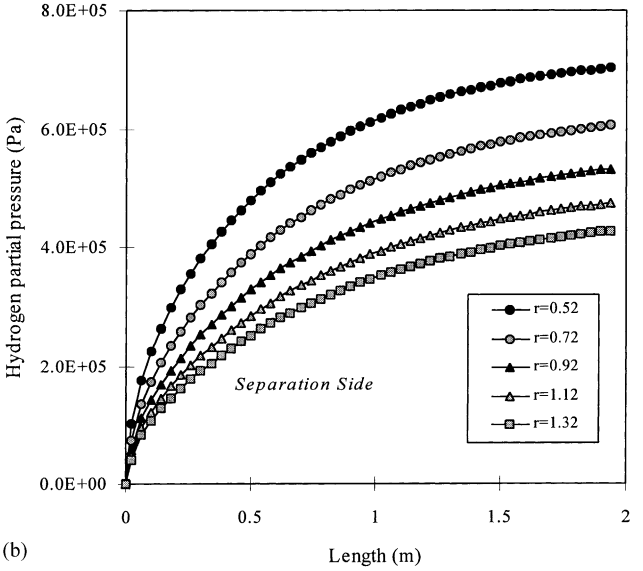

Fig. 5. Axial profiles of hydrogen partial pressure on the separation side for various sweep ratios r for (a) simplified model (inlet specific feed rate $= 1.0\,\mathrm{kg\,m^{-2}\,s^{-1}}$) and (b) dispersion model ($\Phi_R = 0.132$, inlet specific feed rate $= 1.0\,\mathrm{kg\,m^{-2}\,s^{-1}}$).

on this side causing a decrease in hydrogen partial pressure. When dispersion effects are taken into account, smaller values of hydrogen partial pressure are calculated because of the respective decrease of hydrogen fluxes through the membrane (Fig. 5b).

In Figs. 6a and b, predictions of both models for the axial change of the driving force for hydrogen separation are presented for two sweep ratios r. The simplified model predicts a high value of the driving force close to the reactor inlet while later it decreases along the reactor axis (Fig. 6a). Increase in the sweep ratio r results in a corresponding, although small, increase of the hydrogen partial pressure difference. When dispersion conditions are considered, the

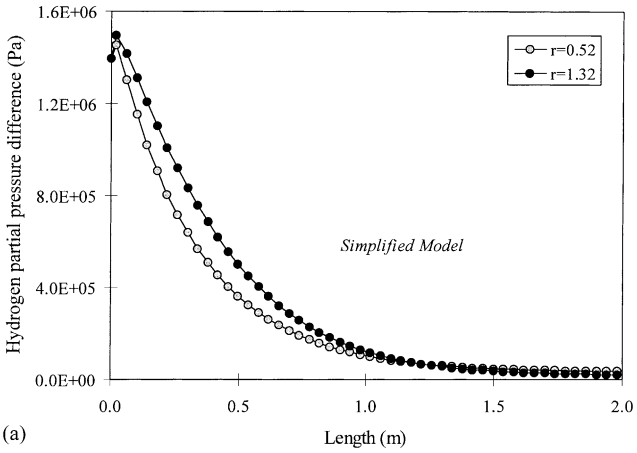

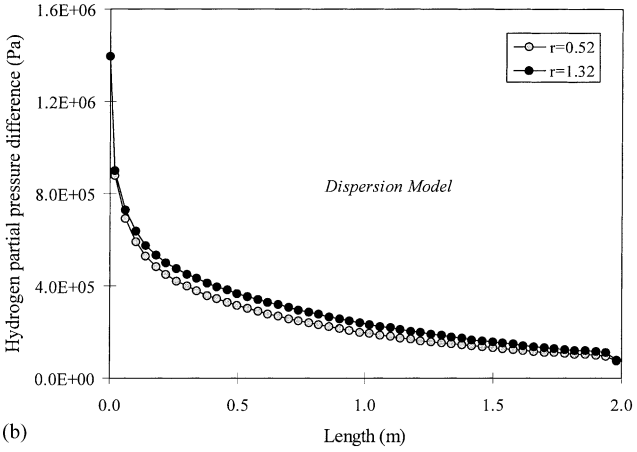

Fig. 6. Axial profiles of driving force for hydrogen separation for two sweep ratios r for (a) simplified model (inlet specific feed rate $= 1.0\,\mathrm{kg\,m^{-2}\,s^{-1}}$) and (b) dispersion model (inlet specific feed rate $= 1.0\,\mathrm{kg\,m^{-2}\,s^{-1}}$).

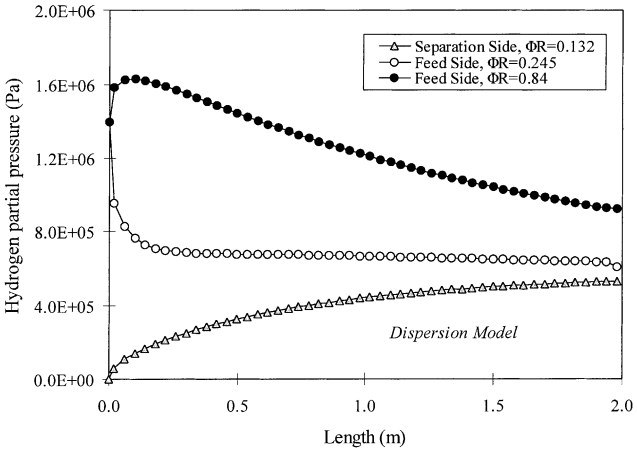

Fig. 7. Axial profiles of hydrogen partial pressure on both sides of the membrane reactor for dispersion model (sweep ratio $r = 0.92$, inlet specific feed rate $= 1.0\,\mathrm{kg\,m^{-2}\,s^{-1}}$.

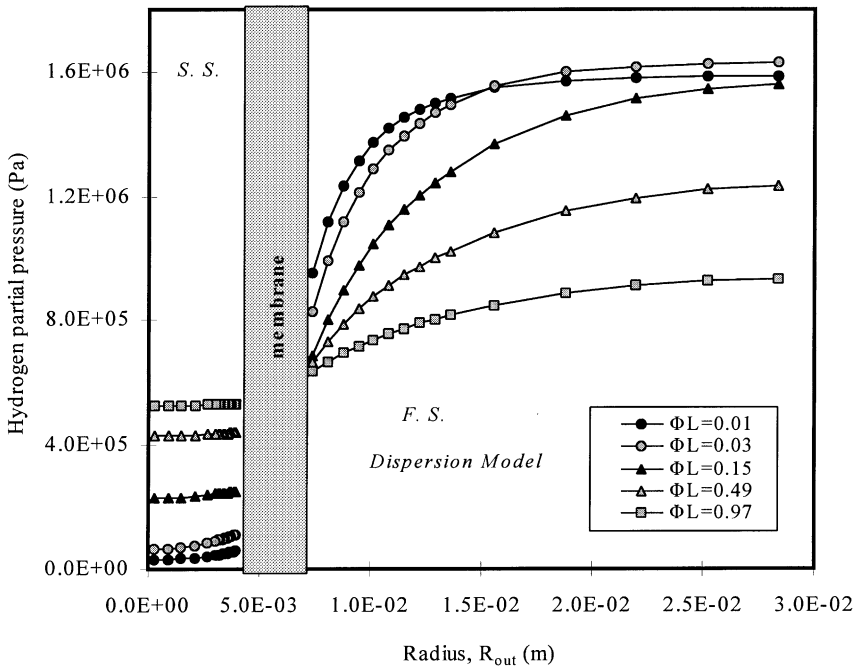

Fig. 8. Radial profiles of hydrogen partial pressure on both sides of the membrane reactor for dispersion model (sweep ratio $r = 0.92$, inlet specific feed rate $= 1.0\,\mathrm{kg\,m^{-2}\,s^{-1}}$). FS: feed side; SS: separation side.

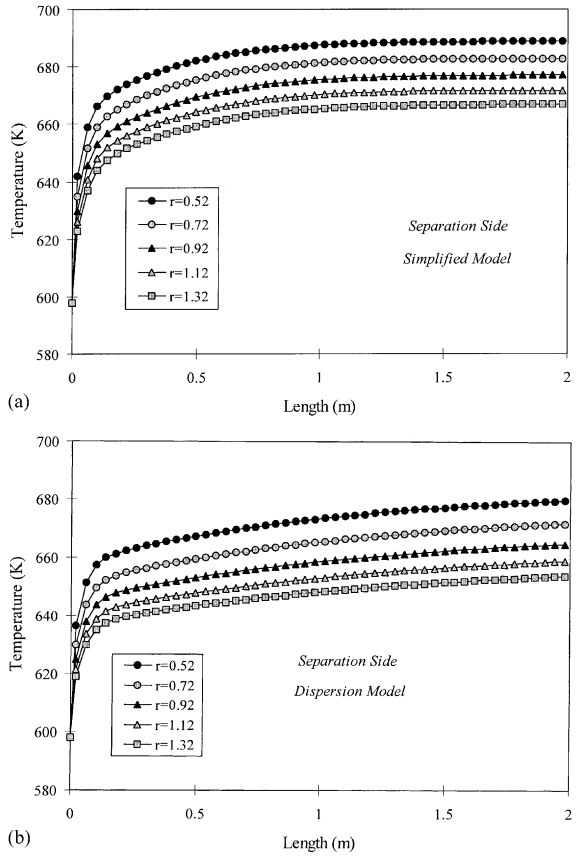

Fig. 9. Axial profiles of temperatures on the separation side for various sweep ratios r for (a) simplified model (inlet specific feed rate $= 1.0\,\mathrm{kg\,m^{-2}\,s^{-1}}$) and (b) dispersion model (inlet specific feed rate $= 1.0\,\mathrm{kg\,m^{-2}\,s^{-1}}$).

driving force for hydrogen separation is low close to the reactor inlet and decreases along the reactor axis (Fig. 6b). The different predictions are attributed to the fact that in the simplified model total radial mixing is assumed without limitations to hydrogen transport along the radius, while for the dispersion model the radially restricted movement of hydrogen accounts for the decreased values of hydrogen partial pressure.

In Fig. 7, axial profiles of hydrogen partial pressure on both sides of the reactor are presented, as they were predicted by the dispersion model. In this case, two axial profiles on the feed side are considered, one profile close to the membrane wall and one close to the wall of the outer tube. These profiles show that under dispersion conditions, hydrogen separation through the membrane influences mainly the area close to the membrane wall ($\Phi_R = 0.245$), while in remote from the wall areas hydrogen partial pressure decreases slowly due to the small radial mass fluxes. In contrast, when plug flow conditions are assumed, separation is affected by a uniform radial distribution, since total radial mixing is assumed (Figs. 4a and 5a).

To get a better insight into the impact of the radial mass transport on the separation process, radial profiles of hydrogen partial pressure predicted by the dispersion model are presented in Fig. 8 for a typical case. In the area close to the reactor inlet, hydrogen is separated quickly through the membrane material because of the high driving force in that area (Figs. 6a and b). Although on the separation side dispersion effects do not greatly affect the variation of the hydrogen partial pressure along the radius, on the feed side they contribute to the formation of even steep radial profiles. It

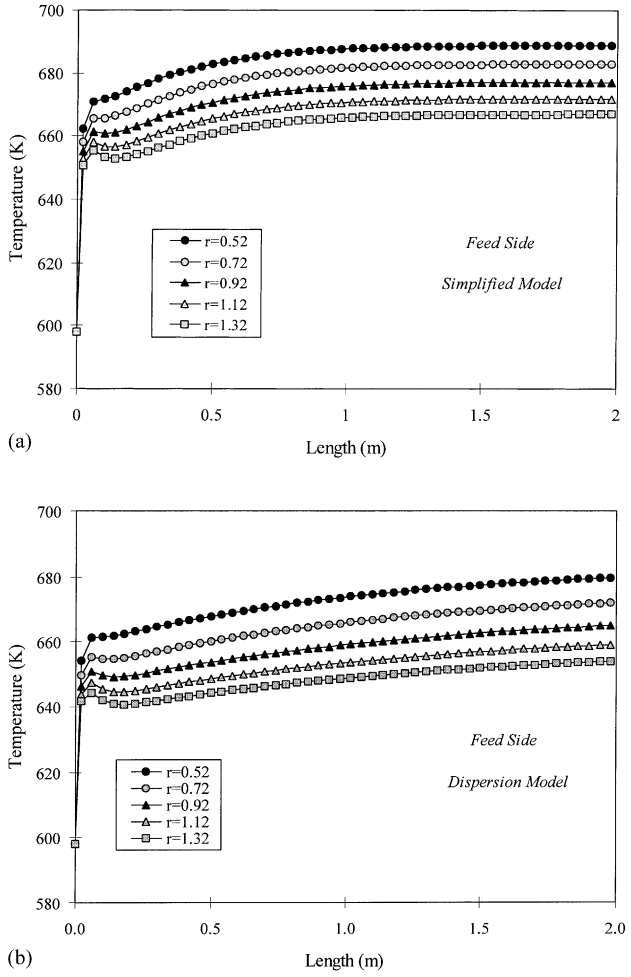

Fig. 10. Axial profiles of temperatures on the feed side for various sweep ratios r for (a) simplified model (inlet specific feed rate $= 1.0\,\mathrm{kg\,m^{-2}\,s^{-1}}$) and (b) dispersion model (inlet specific feed rate $= 1.0\,\mathrm{kg\,m^{-2}\,s^{-1}}$).

is thus obvious that the hydrogen partial pressure increases along the radius and it reaches a maximum in the area close to the outer cylinder wall.

The gradient of the hydrogen partial pressure radial profile is high close to the reactor inlet because of the increased hydrogen production rates, the hydrogen separation through the membrane and the reduced hydrogen radial fluxes calculated by the dispersion model. This gradient decreases along the axis, as hydrogen production rate decreases and hydrogen is transported from the high concentration area, close to the outer wall, to the low concentration area, close to the membrane wall.

In parts a and b of Figs. 9 and 10, axial temperature profiles on both sides of the reactor are presented for various sweep ratios r. As it has already been mentioned, heat, produced by the exothermic reaction, is transferred from the feed side to the separation side. The simplified model predicts an increase of temperature on the separation side along the reactor axis (Fig. 9a) while close to the exit the temperature is very close to the feed side temperature (Fig. 10a). The dispersion model predicts lower temperature values on both sides of the membrane reactor (Figs. 9b and 10b).

5. Conclusions

The present work proposes a mathematical model for the simulation of the performance of an industrial-scale adiabatic membrane reactor. The flow on both sides of the reactor is described by the dispersion model. A simplified model assuming plug flow conditions on both sides of the membrane reactor has been used for the demonstration of the impact of the dispersion effects on the performance of the membrane reactor. Typical results from the application of this mathematical model to the simulation of a membrane reactor, introduced in an integrated gasification combine cycle plant to control carbon dioxide emissions, have been presented.

Dispersion effects result in formation of hydrogen radial profiles and in reduced hydrogen transport rates through the membrane. Radial profiles are very steep close to the membrane reactor inlet. The membrane reactor conversion and the hydrogen recovery predicted by the dispersion model are always much lower than the respective values calculated by the simplified model. It is concluded that, as the dispersion effects may influence the performance of the industrial-scale membrane reactors significantly, especially when highly selective membranes are used, they must be considered as a basic parameter in the design of such reactors.

Acknowledgements

Partial funding for this research work was provided by the European Commission within the framework of the JOULE II and III programmes and this is gratefully acknowledged. Furthermore, the authors would like to express their thanks to CHAM Ltd., London, for permitting the use of their product PHOENICS software.

References

[1] G. Saracco, G.F. Versteeg, W.P.M. van Swaaij, Review: current hurdles to the success of high-temperature membrane reactors, J. Membr. Sci. 95 (1994) 105–123.
[2] J. Zaman, A. Chakma, Review: inorganic membrane reactors, J. Membr. Sci. 92 (1994) 1–28.
[3] J.A. Dalmon, in: G. Ertl, H. Knozinger, J. Weitkamp (Eds.), Handbook of Heterogeneous Catalysis, 1996.
[4] J.N. Armor, Applications of catalytic membrane reactors to refinery products, J. Membr. Sci. 147 (1998) 217–233.
[5] G. Saracco, H.W.J.P. Neomagus, G.F. Versteeg, W.P.M. van Swaaij, High-temperature membrane reactors: potential and problems, Chem. Eng. Sci. 54 (1999) 1997–2017.
[6] M.K. Koukou, N. Papayannakos, N.C. Markatos, Dispersion effects on membrane reactor performance, AIChE J. 46 (9) (1996) 2607–2617.
[7] M.K. Koukou, Mathematical modelling of the performance of membrane reactors–separators, Ph.D. Thesis, National Technical University of Athens, Athens, 1997.

[8] M.K. Koukou, G. Chaloulou, N. Papayannakos, N.C. Markatos, Mathematical modelling of the performance of non-isothermal membrane reactors, Int. J. Heat Mass Transfer 40 (10) (1997) 2407–2417.
[9] M. Bracht, P.T. Alderliesten, R. Kloster, R. Prushek, G. Haupt, E. Xue, J. Ross, M.K. Koukou, N. Papayannakos, Water gas shift membrane reactor for CO_2 control in IGCC systems: techno-economic feasibility study, Energy Conversion Mgmt. 38 (Suppl.) (1997) S159–S164.
[10] M.K. Koukou, N. Papayannakos, N.C. Markatos, M. Bracht, P.T. Alderliesten, Simulation tools for the design of industrial-scale membrane reactors, J. Chem. Eng. Res. Des. Trans. IChemE 76 (Part A) (1998) 911–920.
[11] J.J. Carberry, Chemical and Catalytic Reaction Engineering, McGraw-Hill, New York, 1976.
[12] J. Villermaux, Genie de la Reaction Chimique: Conception et Fonctionnement des Reacteurs, 2nd Edition, Tec and Doc, Lavoisier, 1993.
[13] N.C. Markatos, Computational fluid flow capabilities and software, Ironmaking and Steelmaking 16 (1989) 266.
[14] N.C. Markatos, Mathematical modelling of single- and two-phase flow problems in the process industries, Revue de l' Institut Francais du Petrole 48 (6) (1993) 631.
[15] D.B. Spalding, Mathematical Modelling of Fluid Mechanics, Heat Transfer and Chemical Reaction Processes, Lecture Course, HTS/80/1, Imperial College, London, 1980.
[16] R.B. Bird, W.E. Stewart, E.N. Lightfoot, Transport Phenomena, Wiley, New York, 1960.
[17] P.P.A.C. Pex and The ECN Gas Separation Group, Materials aspects of microporous inorganic gas separation membrane manufacturing, in: W.R. Bowen, et al. (Ed.), Proceedings of the Euromembrane '95, Bath, Vol. 1, 1995, pp. 295–300.
[18] S.R. Tennison, Microporous ceramic membranes for gas separation processes, Final Technical Report, EC Project JOE3-CT95-0018, 1998.
[19] R.L. Keiski, T. Salmi, V.J. Pohjola, Development and verification of a simulation model for a non-isothermal water gas shift reactor, Chem. Eng. J. 48 (1992) 17–29.
[20] E.J. Henley, J.D. Seader, Equilibrium-stage Separation Operation in Chemical Engineering, Wiley, New York, 1968.
[21] R.H. Perry, D. Green, Perry's Chemical Engineers' Handbook, 6th Edition, McGraw-Hill, New York, 1986.
[22] W.D. Kinjery, H.K. Bowen, D.R. Uhlmann, Introduction to Ceramics, Wiley, New York, 1976.